





cently analyzed by Haller and Liu,<sup>15</sup> who showed that they result from the attraction of the concentration field to a time-dependent inertial manifold that is spanned by a finite number of strange eigenmodes. Using standard energy estimates, they establish critical straining rates (Peclet numbers) below which such structures cannot exist. Several examples of model flows are given.

A related work is that of Saadjan and Leprevost.<sup>16</sup> Commenting on the fact that chaotic mixing and transport enhancement are closely related, they treated the problem of transport in the annular region between confocal ellipses whose surfaces are held at different temperatures and are assumed to glide without changing the orientation of the ellipse relative to fixed coordinates, allowing them to solve the transport problem on a fixed domain. Most of the focus is on the case of time-modulated surface velocity and attempts to correlate the transport rates with the mixing zone approach of Kaper and Wiggins.<sup>17</sup> Although their parametric study is limited, the authors do comment that there is an optimal frequency of modulation that maximizes the transport.

### C. Transport from drops in unsteady flow

Turning now to the specific case of transport from droplets in unsteady flows, Lee *et al.*<sup>18</sup> were, to our knowledge, the first to consider the effects of modulation of the electric field on transport rates. Although their paper is primarily focused on steady nonuniform electric fields (and therefore the computation of the dielectrophoretic velocity), they recognized the possibility of driving chaotic advection with time-varying electric fields and presented some Poincaré sections that demonstrated this. They also presented solutions to the convective diffusion equation for such chaotic flows for a very limited range of parameters. Although they computed the transport enhancement in a complicated and nonstandard way, and the conditions under which their results apply are not clear, they observed a nonmonotonic dependence of the enhancement on frequency. We will discuss their work in more detail below.

In a sequence of two papers, Ward and Homsy<sup>19,20</sup> studied chaotic advection in uniform time-modulated electric fields and included the important effects of a steady translation velocity. They showed how the modulation of the electric field results in excursions of the location of the stagnation disk shown in Fig. 1, and that the cycling of the flow fields among the patterns shown there results in trajectory splitting and chaotic advection. Mixing was characterized by calculating the percentage of the drop volume that contained chaotic trajectories. Their results, Fig. 2 of Ref. 20, show that the mixed volume increases linearly with frequency for small frequency, decays exponentially fast at high frequency, and exhibits a large broadband plateau over 1–2 decades of intermediate frequencies. Furthermore, it is possible to find parameters for which essentially all of the drop is mixed. The first two of these features are in agreement with the general considerations of Refs. 8 and 9, but leave open the issue of the rate of heat mass transfer from such chaotically stirred drops.

### D. Objectives

We have seen that in the case of unsteady flows resulting in chaotic advection, quantitative predictions of the enhancement in transport rate for realistic flows are few, the dependence of the enhancement on frequency is, in general, difficult to obtain, the range of parameters covered is usually small, and the mechanisms responsible for the enhancement remain poorly understood. The problem undertaken here—transport from droplets with time-dependent internal circulations—is an attractive context in which to study these issues since

- the flow fields are analytically determined;
- the transport problem for steady flow fields is classical and well understood in certain limits;
- generic features such as filamentation of material elements by folding and stretching are present; and
- the problem represents one that is in principle experimentally realizable.

Thus our objectives are to provide as thorough a set of predictions of the rates of heat or mass transfer from circulating drops as possible. We treat both steady and modulated electric fields. Section II gives the problem formulation, the scalings, and the parameters of the problem. Section III presents the numerical method and Sec. IV contains various validation studies of it. Section V presents results for steady settling and steady electric field over a wide range of  $Pe$  and  $W$ , thus completing a full set of predictions for the problem originally posed by Chang *et al.*<sup>5</sup> It is found, in accord with the general considerations of Pan and Acrivos,<sup>4</sup> that transport remains diffusion limited, but the enhancement factor due to the Taylor circulation can be as large as 4.5. Time modulated electric fields are treated in Sec. VI, in which case the parameter space is enlarged by two additional parameters; the dimensionless frequency and the value of  $W$  corresponding to the time-dependent part of the electric field. Various parametric studies are conducted and nonintuitive scalings are discerned from a very large set of results. Most interestingly, the enhancement factor is seen to be nonmonotonic in the frequency, and the explanation of this effect is pursued through visualizations of the concentration fields presented in Sec. VII. Section VIII contains a discussion of the results in the context of previous work and our conclusions.

## II. PROBLEM FORMULATION

Consider the convective diffusion equation for scalar  $c$ , which we refer hereafter to as “the concentration,” although it also governs the temperature in the case of heat transfer,

$$\frac{\partial c}{\partial t} + \text{Pe} \, \bar{v} \cdot \nabla c = \Delta c. \quad (1)$$

The variables are made dimensionless by a certain characteristic velocity  $\bar{U}$ , the drop radius  $a$ , the initial concentration  $c_0$ , and the diffusion coefficient,  $D$ . The time is scaled by the diffusion scale  $aD^{-2}$  and  $\text{Pe} = a\bar{U}/D$ . Since the flow is axisymmetric, we consider spherical coordinates  $\theta \in [0, \pi]$ ,  $r \in [0, 1]$  for which  $\theta=0$  and  $\theta=\pi$  are the rear, and forward

stagnation points, respectively. Hence the equation governing the concentration of the solute is

$$\frac{\partial c}{\partial t} + \text{Pe} \left( v \frac{\partial c}{\partial r} + w \frac{\partial c}{\partial \theta} \right) = \frac{\partial c}{\partial r^2} + \frac{2}{r} \frac{\partial c}{\partial r} + \frac{1}{r^2 \sin \theta} \frac{\partial}{\partial \theta} \sin \theta \frac{\partial c}{\partial \theta}. \quad (2)$$

Here  $v$  and  $w$  stand for the radial,  $u_r$ , and polar,  $u_\theta$ , components of velocity, respectively. Some of the validation studies will include a source term  $F(r, \theta)$  in Eq. (2). The velocity components are related to the stream function of the flow as follows:

$$v \equiv u_r = \frac{1}{r^2 \sin \theta} \frac{\partial \psi}{\partial \theta}, \quad w \equiv u_\theta = -\frac{1}{r \sin \theta} \frac{\partial \psi}{\partial r}.$$

In the present work we consider a superposition of two flows, with stream functions  $\psi^B$  and  $\psi^E$ , and (dimensionless) characteristic velocities  $U$  and  $V$ , respectively. Then

$$\psi = U\psi^B + V\psi^E.$$

Now  $\psi^B$  is the stream function of the flow with constant velocity at infinity, i.e., the Hadamard–Rybczynski flow, the expression for which reads

$$\psi^B = \frac{1}{2}(r^4 - r^2)\sin^2 \theta.$$

Here the factor  $\frac{1}{2}$  normalizes the maximum dimensionless velocity at the sphere surface. The sign of the stream function reflects the fact that the radial component of the flow is negative at the top,  $\theta = \pi$ , the flow at infinity being upward.

As discussed, the flow given by  $\psi^E$  is known as the Taylor flow and represents the velocity distribution due to a flow with a constant gradient at infinity given by

$$\psi^E = (r^3 - r^5)\sin^2 \theta \cos \theta.$$

Once again a numerical factor is selected such that its maximum velocity at the drop surface is equal to unity. For the velocity components we get

$$-\frac{1}{r \sin \theta} \frac{\partial \psi^B}{\partial r} = -\frac{1}{2}(4r^2 - 2)\sin \theta, \quad (3)$$

$$-\frac{1}{r \sin \theta} \frac{\partial \psi^E}{\partial r} = -(3r - 5r^3)\sin \theta \cos \theta, \quad (4)$$

$$\frac{1}{r^2 \sin \theta} \frac{\partial \psi^B}{\partial \theta} = (r^2 - 1)\cos \theta, \quad (5)$$

$$\frac{1}{r^2 \sin \theta} \frac{\partial \psi^E}{\partial \theta} = (r - r^3)(2 \cos^2 \theta - \sin^2 \theta), \quad (6)$$

which give

$$w = -U(2r^2 - 1)\sin \theta - V(3r - 5r^3)\sin \theta \cos \theta, \quad (7)$$

$$v = U(r^2 - 1)\cos \theta + V(r - r^3)(2 \cos^2 \theta - \sin^2 \theta). \quad (8)$$

With the flow thus defined, the question of choice of the characteristic velocity  $\bar{U}$  arises, and the natural thing would

be to take it as the maximum speed, which occurs on the surface. The detailed expression for  $\max|w(r=1, \theta)|$  as function of  $U, V$  is tedious but we can show that  $\max|\bar{v}| \equiv \max|w|$ . There is only 20% difference between the actual value of  $\max|w|$  and  $\leq \sqrt{U^2 + V^2}$ , and only when  $U$  and  $V$  are of the same order of magnitude. Thus we take  $\bar{U} = \sqrt{U^2 + V^2}$  which allows us to cover the case of stationary and translating drops without changing the scaling. In addition, our experience shows that this choice allows the most convenient presentation of results. For the sake of comparison with previous work we also introduce the dimensionless ratio of the amplitudes of these two flows, namely,

$$W \stackrel{\text{def}}{=} \frac{V}{U},$$

which governs the relative importance of the gradient flow.

In the present work we consider steady translation of the drop but allow the amplitude of the gradient flow to vary in time with dimensional frequency  $\omega'$ . Thus

$$W = W_1 + W_2 \cos(\Omega t),$$

where  $\Omega = \omega' a^2 / D$  is the frequency made dimensionless by the diffusion time scale. Thus in this case the velocities depend on both space and time.

The boundary conditions for the concentration stem from the assumption that the transport is controlled by diffusion in the dispersed phase. Then one can assume that the concentration at the drop surface relaxes instantaneously due to the fast diffusion in the continuous phase. Hence the concentration is constant at the boundary, which without loss of the generality we set to zero, i.e.,

$$c(r, \theta) = 0, \quad r = 1, \quad \theta \in [0, \pi]. \quad (9)$$

The spherical symmetry requires that a smooth function has zero derivatives at the poles of the drop, namely,

$$\frac{\partial c}{\partial \theta} = 0, \quad \theta = 0, \pi, \quad (10)$$

and at the origin of the coordinate system,

$$\frac{\partial c}{\partial r} = 0, \quad r = 0. \quad (11)$$

We also assume that the initial dimensionless concentration is homogeneous and equal to unity, i.e.,

$$c(r, \theta, t = 0) = 1.$$

### III. NUMERICAL METHOD

The aim of the present work is to examine the unsteady transport for moderate and large Peclet numbers. Equation (2), although linear, has coefficients which, in general, vary both in space and time and therefore must be solved numerically. When the Peclet number is large, the advective terms tend to dominate the diffusion terms and the accuracy of the numerical scheme is governed by the so-called grid Peclet number,  $\text{Pe}_h = h\text{Pe}$ , where  $h = \max\{h_\theta, h_r\}$  and  $h_\theta, h_r$  are the spacings defined in what follows. We used an implicit

scheme with central differences with measures taken to secure its stability, employing both a staggered grid and a special approximation of the advective terms.

### A. Grid and spatial approximations

We choose staggered grids both in  $r$ - and  $\theta$ -directions, namely,

$$r_i = h_r \left( i - \frac{1}{2} \right), \quad h_r = \frac{1}{M - \frac{1}{2}}, \quad (12)$$

$$\theta_j = h_\theta \left( j - \frac{1}{2} \right), \quad h_\theta = \frac{\pi}{N}, \quad (13)$$

where  $M$  and  $N$  are the numbers of points in the  $r$ - and  $\theta$ -directions. Clearly  $i=1$  corresponds to points situated on distance  $h_r/2$  from the singularity point, while  $i=M$  gives the surface of the drop,  $r=1$ .

The various differential operators are approximated as follows:

$$\begin{aligned} \Lambda_r \Phi_{i,j} &\stackrel{\text{def}}{=} v_{i+(1/2),j}^{n+(1/2)} \frac{\Phi_{i+1,j} - \Phi_{i,j}}{2h_r} + v_{i-(1/2),j}^{n+(1/2)} \frac{\Phi_{i,j} - \Phi_{i-1,j}}{2h_r} \\ &\approx v(r, \theta) \frac{\partial \Phi}{\partial r} + O(h_r^2), \end{aligned} \quad (14)$$

$$\begin{aligned} \Lambda_\theta \Phi_{i,j} &\stackrel{\text{def}}{=} w_{i,j+(1/2)}^{n+(1/2)} \frac{\Phi_{i,j+1} - \Phi_{i,j}}{2r_i h_\theta} + w_{i,j-(1/2)}^{n+(1/2)} \frac{\Phi_{i,j} - \Phi_{i,j-1}}{2r_i h_\theta} \\ &\approx \frac{w(r, \theta)}{r} \frac{\partial \Phi}{\partial \theta} + O(h_\theta^2), \end{aligned} \quad (15)$$

$$\begin{aligned} \Lambda_{rr} \Phi_{i,j} &\stackrel{\text{def}}{=} \frac{r_{i+(1/2)}^2}{r_i^2 h_r^2} \Phi_{i+1,j} - \left[ \frac{r_{i+(1/2)}^2}{r_i^2 h_r^2} + \frac{r_{i-(1/2)}^2}{r_i^2 h_r^2} \right] \Phi_{i,j} \\ &\quad + \frac{r_{i-(1/2)}^2}{r_i^2 h_r^2} \Phi_{i-1,j} \approx \frac{1}{r^2} \frac{\partial}{\partial r} r^2 \frac{\partial \Phi}{\partial r} + O(h_r^2), \end{aligned} \quad (16)$$

$$\begin{aligned} \Lambda_{\theta\theta} \Phi_{i,j} &\stackrel{\text{def}}{=} \frac{\sin(\theta_{j+(1/2)})}{r_i^2 \sin(\theta_j) h_r^2} \Phi_{i,j+1} - \left[ \frac{\sin(\theta_{j+(1/2)})}{r_i^2 \sin(\theta_j) h_r^2} \right. \\ &\quad \left. + \frac{\sin(\theta_{j-(1/2)})}{r_i^2 \sin(\theta_j) h_r^2} \right] \Phi_{i,j} + \frac{\sin(\theta_{j-(1/2)})}{r_i^2 \sin(\theta_j) h_r^2} \Phi_{i,j-1} \\ &\approx \frac{1}{r^2 \sin \theta} \frac{\partial}{\partial \theta} \sin \theta \frac{\partial \Phi}{\partial \theta} + O(h_\theta^2). \end{aligned} \quad (17)$$

The benefits of using the staggered grid become clear. The three-point differences for the second-order derivatives become effectively two-point relationships at the singularity of the coordinate system because  $r_{1/2}=0$  and  $\sin(\theta_{1/2})=\sin(0)=0$ ,  $\sin(\theta_{N+(1/2)h_\theta})=\sin(\pi)=0$ . Thus no special boundary conditions have to be imposed at the singularity line. Yet there is a condition for smoothness,  $\partial c / \partial r=0$ , of the concentration profile at the singularity point ( $r=0$ , any  $\theta$ ). A similar requirement,  $\partial c / \partial \theta=0$ , holds at  $\theta=0, \pi$ . The condition on the  $r$ -derivative gives

$$c_{0,j} = c_{1,j},$$

which completes the difference approximation  $\Lambda_r$  as follows:

$$\Lambda_r \Phi_{1,j} \stackrel{\text{def}}{=} v_{(3/2),j}^{n+(1/2)} \frac{\Phi_{2,j} - \Phi_{1,j}}{2h_r}.$$

Thus the values,  $c_{0,j}$ , which lie outside the chosen grid, can be replaced in the difference approximation by the values  $c_{1,j}$ . The requirements on the  $\theta$ -derivative give similar difference conditions

$$c_{i,0} = c_{i,1} \quad \text{and} \quad c_{i,N+1} = c_{i,N-1},$$

but they are not really needed because in the  $\theta$ -component of velocity,  $w$  is equal to zero at the singularity line due to the symmetry of the problem, in contrast with the case of the  $r$ -component.

Following Ref. 21 we can prove that the special differencing for the first-order operators used above is conservative in the sense that

$$\langle \Phi, \Lambda_r \Phi \rangle = 0 \quad \text{and} \quad \langle \Phi, \Lambda_\theta \Phi \rangle = 0 \quad (18)$$

for a standard difference scalar product  $\langle \cdot, \cdot \rangle$ . Hence the norm of  $c$  cannot increase in time. Theoretically this means that the scheme is stable but it should not be used with very large time increments for large Peclet numbers because then accuracy is lost.

### B. Time stepping by operator splitting

Denote for brevity

$$\Lambda_1 = -\Lambda_r + \Lambda_{rr} \quad \text{and} \quad \Lambda_2 = -\Lambda_\theta + \Lambda_{\theta\theta}.$$

Our time-stepping method is of the Crank–Nicholson type

$$\frac{c_{i,j}^{n+1} - c_{i,j}^n}{\tau} = \Lambda_1 \frac{c_{i,j}^{n+1} + c_{i,j}^n}{2} + \Lambda_2 \frac{c_{i,j}^{n+1} + c_{i,j}^n}{2}, \quad (19)$$

which approximates the original differential equation to  $O(\tau^2)$  but requires the inversion of very large block-diagonal matrices. To circumvent this, we use the following operator-splitting scheme:

$$\left[ I - \frac{\tau}{2} \Lambda_2 \right] \hat{c}_{i,j} = \left[ I + \frac{\tau}{2} \Lambda_2 \right] \left[ I + \frac{\tau}{2} \Lambda_1 \right] c_{i,j}^n, \quad (20)$$

$$\left[ I - \frac{\tau}{2} \Lambda_1 \right] c_{i,j}^{n+1} = \hat{c}_{i,j}, \quad (21)$$

where  $I$  is the identity matrix. Thus our method consists of advancing the solution in two fractional steps, each of which is implicit in time and one of the spatial variables. Thus the method is in the spirit of multidimensional Crank–Nicholson/alternating-directions-implicit methods.

Eliminating the intermediate variable  $\hat{c}$  gives

$$\begin{aligned} \frac{c_{i,j}^{n+1} - c_{i,j}^n}{\tau} &= \Lambda_1 \frac{c_{i,j}^{n+1} + c_{i,j}^n}{2} + \Lambda_2 \frac{c_{i,j}^{n+1} + c_{i,j}^n}{2} \\ &\quad + \frac{\tau^2}{4} \Lambda_1 \Lambda_2 \frac{c_{i,j}^{n+1} - c_{i,j}^n}{\tau}, \end{aligned} \quad (22)$$

which approximates Eq. (19) to  $O(\tau^2)$ .

As already mentioned, the difference approximations of the advective terms are antisymmetric operators. Then both  $\Lambda_1$  and  $\Lambda_2$  are negative operators which makes the operators  $I - (\tau/2)\Lambda_i$  of norm greater than one, or  $\|I - (\tau/2)\Lambda_i\|^{-1} < 1$  [see Eq. (18)]. This secures the unconditional stability of the scheme for the full time step. However, since the scheme employs operator splitting and since the operators in spherical coordinates do not commute, it cannot be proved strictly that the stability of the transition from one fractional step to another is unconditional, but the size of the time step can be fairly large and still maintain stability. This means that the selection of the scheme parameters (time increment and grid spacings) can be based solely on physical considerations.

#### IV. VALIDATION STUDIES

Validation studies were done with different spatial and/or temporal resolutions in order to verify the accuracy of the scheme. For the range of parameters covered we found that fully adequate results can be obtained on a grid with  $M \times N = 81 \times 240$  points. In some special cases we used finer meshes as discussed below. The rationale for selecting this specific ratio between the number of grid lines in the two directions is that in the  $\theta$ -direction the length is  $l_\theta = \pi \approx 3$ , while in the  $r$ -direction the length is equal to one. Hence taking three times more points in the  $\theta$ -direction ensures that  $h_r$  and  $h_\theta$  are roughly equal.

##### A. Spatial approximation

The simplest test to assess the accuracy of spatial differencing is to set the advection velocities equal to zero and to augment Eq. (2) with a source term  $F(r, \theta) \equiv 1$ . Starting from an arbitrary initial condition the scheme should reproduce the analytical solution with spherical symmetry, namely,  $c(r, \theta) = \frac{1}{6}(1 - r^2)$ . Time integration to steady state resulted in a difference between the numerical solution and this analytical expression of less than 0.1% on the  $81 \times 240$  grid. A further validation is provided by the analytical solution of the stationary problem without spherical symmetry when the source also lacks this symmetry: A convenient test case is

$$F(r, \theta) = \cos \theta \quad \text{for which} \quad c(r, \theta) = \frac{1}{4}r(1 - r)\cos \theta.$$

In this case, the difference between the numerical results at long times and the analytical solution was of the order of 0.2%. One final case is needed to validate the accuracy of the approximation for the advective terms. Consider a case with  $v(r, \theta) = 1/r$ ,  $w(r, \theta) = 0$ , and  $F = 1$ . This is a very harsh test since the velocity component  $v$  has a singularity at the origin. Equation (2) reduces to

$$\frac{1}{r} \frac{dc}{dr} = \frac{d^2c}{dr^2} + \frac{2}{r} \frac{dc}{dr} + 1,$$

whose analytical solution is  $\frac{1}{4}(1 - r^2)$ : The numerically obtained field at long times differed from the above expression by 0.21%. Finally, the error on different grids was observed to be consistent with the second-order spatial approximation, i.e., when refining the mesh by a factor of 2, the error decreased fourfold. These tests suffice to show that the stag-

gered spatial difference approximation that we use for the second-order operators provides high accuracy.

##### B. Temporal approximation

There is a well-known solution to the diffusion equation, i.e.,  $Pe = 0$ , that involves the sinc function and decays asymptotically with time,

$$c(r, \theta; t) = \frac{\sin(\pi r)}{\pi r} e^{-\pi^2 t}. \quad (23)$$

We conducted a validation study by using Eq. (23) evaluated at  $t = 0$  as the initial condition and then monitoring the numerically computed average concentration with time. Our calculations confirmed the decay constant of  $\pi^2$  within the truncation error  $O(h_r^2 + h_\theta^2 + \tau^2)$ . Moreover, the profile after a short transient was precisely equal to Eq. (23) within the same order of approximation.

##### C. The extraction time

In order to track the behavior of the concentration with time we consider the total amount of solute in the drop at time  $t$ , normalized by its initial value. For the initial condition  $c^0 \equiv 1$ ,

$$\begin{aligned} \langle c \rangle^n &= \frac{3}{4\pi} \int_0^{2\pi} \int_0^1 \int_0^\pi c(r, \theta, t^n) r^2 \sin \theta dr d\theta d\phi \\ &= \frac{3}{2} \int_0^1 \int_0^\pi c(r, \theta, t^n) r^2 \sin \theta dr d\theta \\ &= \frac{3}{2} h_r h_\theta \sum_{j=1}^N \left[ \sum_{i=1}^{M-1} r_i^2 c_{i,j}^n + \frac{1}{2} (r_{M-1}^2 c_{M-1,j}^n + r_M^2 c_{M,j}^n) \right] \sin \theta_j \\ &\quad + O(h_r^2 + h_\theta^2), \end{aligned}$$

where  $n$  denotes the corresponding time step. The numerical quadrature used in the above formula is a midpoint approximation in the  $\theta$  direction. Singling out the last point in the  $r$ -direction is necessary because of the specific pattern of the grid: At  $r = 0$  it is staggered, while at  $r = 1$  it fits the boundary. Note that the grid is given by Eqs. (12) and (13), and that for the case under consideration,  $c_{M,j}^n = 0$  due to the boundary conditions. One has  $\langle c^0 \rangle = 1$  and one expects exponential decay of this quantity with time.

As is well known,<sup>1-3</sup> after an initial stage of adjustment, the time dependence of  $\langle c \rangle$  settles to an exponential decay described by

$$\langle c \rangle = A e^{-\alpha \pi^2 t}, \quad (24)$$

where  $\alpha \pi^2$  is the decay constant called  $\lambda$  in Ref. 22 and earlier works. Hence  $\alpha = 1$  is the case of pure diffusion. We refer to  $\alpha$  as the ‘‘enhancement factor’’ and present our results in terms of its dependence on the different parameters of the problem.

The most natural way to get the value of  $\alpha$  from the numerical results is to consider the ratio between the average concentration at two consequent time steps, namely,

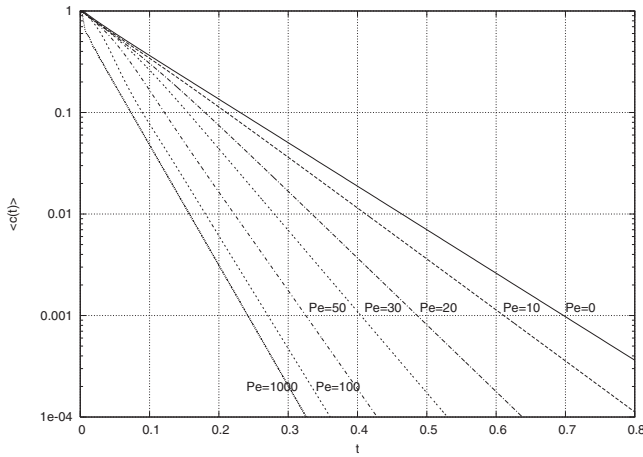


FIG. 2. Decay of the total mass as function of time for Hadamard flow for different Peclet numbers. The results for  $Pe=2000$  and  $Pe=4000$  are not shown because they virtually overlap those for  $Pe=1000$ .

$$f^n = \frac{\langle c^n \rangle}{\langle c^{n+1} \rangle}.$$

Then an asymptotic behavior will be reached in which

$$\lim_{n \rightarrow \infty} f^n = F = e^{\alpha \tau \pi^2},$$

or equivalently,

$$\alpha = \frac{\ln F}{\tau \pi^2}, \quad (25)$$

where  $\tau$  is the time increment.

For steady flows,  $\alpha$  is constant, while for periodic flows one has to generalize Eq. (24) as

$$\langle c \rangle = B \cos(\omega t + \gamma) e^{-\alpha \pi^2 t}, \quad (26)$$

where  $\gamma$  is a phase angle. Thus for the modulated flow, the enhancement factor is a function of  $t$  and the numerical value from Eq. (25) is a function of  $n$ . As already discussed above, after a short transient the regime settles to a decaying oscillation of the form of Eq. (26).

Figure 2 shows the calculated total mass as a function of time for  $W=0$  (Hadamard circulation) for different Peclet numbers. It is clear that except for a short initial transient, Eq. (24) is valid and the slope of the curves in the figures gives the enhancement factor  $\alpha$ .

The final verification of the scheme is provided by comparison of the extraction time for the extreme case of very large Peclet number for the Hadamard flow. Kronig and Brink<sup>1</sup> used a special coordinate system and solved this problem semianalytically. They found that after an initial transient, the concentration field is close to the first eigenfunction (the others having much larger decay constants) and the mass depends on time as  $e^{-\lambda_1 t}$ , where  $\lambda_1$  is the first (smallest) eigenvalue of their transformed problem. The value  $\lambda_1$  given in Ref. 1 was later verified and refined (see Ref. 22) and can safely be assumed to be equal to  $\lambda_1 = 2.718 \pi^2$ . In order to compare with that value we ran calculations with different spatial resolutions. Naturally the value obtained depended on the resolution and varied proportionally to the order of trun-

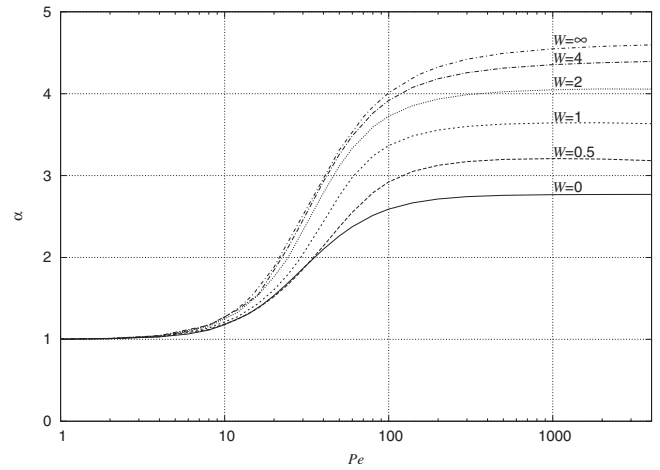


FIG. 3. Dependence of the enhancement factor  $\alpha$  on Peclet number  $Pe$ .

cation error: On coarser meshes it tended to be larger. The finest mesh we employed was a  $161 \times 480$  grid. Our results for  $Pe=2000$  and  $Pe=4000$  are indistinguishable from each other and both give  $\lambda = 2.764 \pi^2$ , which agrees with the accepted value<sup>22</sup> to within 2%.

## V. RESULTS FOR THE STEADY HADAMARD-TAYLOR PROBLEM

We begin with pure Hadamard flow which corresponds to the case  $U=1$ ,  $V=0$ . Figure 2 shows the evolution of the total mass with time for seven different Peclet numbers from which the enhancement factor may be calculated. As already discussed, the slope of the curve  $Pe=0$  is virtually equal to  $-\pi^2$  and that for very large  $Pe$  the slope is  $-2.764 \pi^2$ . We next treat the steady combined Hadamard-Taylor flow. We chose  $U=1$ ,  $V=W$  and treat  $W$  as an additional parameter. Results similar to those in Fig. 2 (not shown) were obtained for a range of  $W$ . Figure 3 shows the dependence of the enhancement factor  $\alpha$ , on  $Pe$  for different  $W$  up to  $Pe=4000$ . A comment is required regarding the definition of  $Pe$ . As already mentioned in Sec. II, the characteristic velocity of the Hadamard-Taylor flow was taken as  $\sqrt{U^2 + V^2}$  and this velocity is the one used to compute  $Pe$  in Fig. 3. Since the maximum velocity of the flow is only roughly approximated by this quantity, there are slight intersections of the curves for  $W=0$  and  $W=0.5$ .

The lowest curve in Fig. 3 corresponds to the pure Hadamard flow and is therefore derived from the results in Fig. 2. Our results cover a wide range of  $Pe$  and are in good agreement with previous results available over a smaller range of  $Pe$ . In particular, they agree with both the intuitive curve drawn by Johns and Beckmann<sup>2</sup> and their limited numerical results. They also agree with those of Bryden and Brenner<sup>3</sup> when slight differences between their interfacial boundary condition for the concentration and the one used here are taken into account.

One sees that the presence of a stationary circulation in the translating drop leads to an enhancement factor that asymptotes to  $\alpha \approx 2.8$  as  $Pe \rightarrow \infty$ . On the other hand, pure Taylor flow,  $W \rightarrow \infty$ , is more efficient and gives enhancement

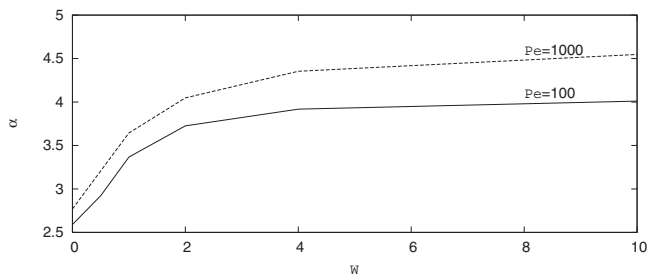


FIG. 4. Dependence of the enhancement factor  $\alpha$  on  $W$  for two different Peclet numbers.

factors as large as  $\alpha \approx 4.6$ . Naturally, the different combinations of the two flows yield enhancement factors that fall between these two limits. The enhancement factor changes rapidly for small  $W < 1$ : When  $W = 1$  the enhancement factor is already half way to its value for  $W = \infty$ . This means that a Taylor flow component with even a moderate amplitude has a significant impact on the mass transfer. This effect is depicted in a cross plot, Fig. 4, where the dependence of  $\alpha$  on  $W$  is shown for  $Pe = 100$  and  $Pe = 1000$ . Clearly, the qualitative dependence of  $\alpha$  on  $W$  is similar for moderate and large Peclet numbers. This is in turn related to the fact that a second vortex appear when  $W > 0.5$ , as shown in Fig. 1 and discussed above. This second vortex decreases the distance over which diffusion must act, which accounts for the increase in  $\alpha$ .

It is expected that for large  $Pe$ , i.e., convection-dominated situations, the curves of constant concentration (isopleths) should conform to the streamlines because the passive scalar is advected with the flow velocity and diffusion is too slow to significantly change the concentration along a streamline.<sup>1</sup> Figure 5 presents a comparison between the streamlines and isopleths for  $Pe = 2000$  using a so-called density plot (in which the isopleths are the imaginary lines separating different gray levels). As can be seen, the two fields are near identical, thus confirming these expectations.

It is seen that  $\alpha$  changes most rapidly for  $10 \leq Pe \leq 100$  for all  $W$ . The plateaus beyond  $Pe > 100$  implies that

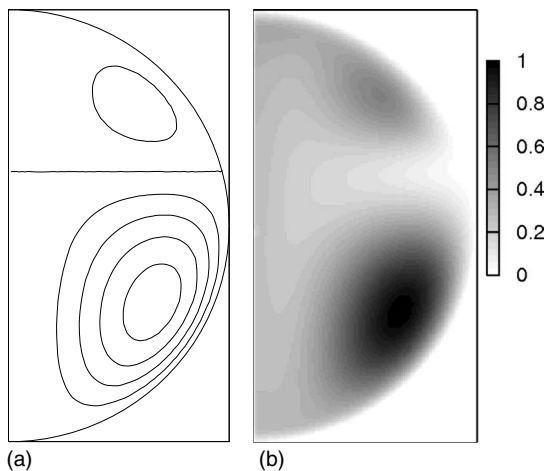


FIG. 5. Stream function (left panel) and normalized concentration (right panel) for the Hadamard-Taylor flow with  $W = 2$ .

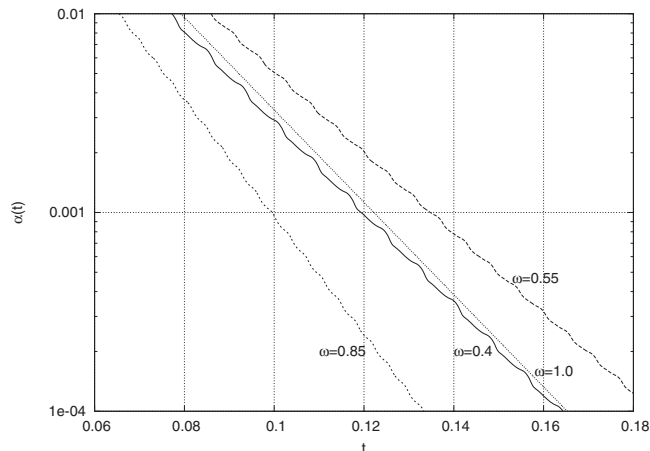


FIG. 6. Time dependence of the concentration for  $W = 10$ ,  $\delta = 0.9$ , and  $Pe = 2000$ .

the large Peclet number regime begins around  $Pe = 200$ . The conclusion of this section is that increasing either  $Pe$  or  $W$  acts to speed up the process of extraction but that for steady flows, transport remains limited by cross-streamline diffusion as expected.

## VI. RESULTS FOR THE PULSATILE FLOW PROBLEM

### A. Preliminaries

In terms of the above defined dimensionless variables the stream function is given by

$$\psi = \psi^B + W\psi^E, \quad \text{where} \quad W = \frac{V}{U} = W_1 + W_2 \cos(\Omega t).$$

We will present the results in terms of  $\omega = \omega'(a/\bar{U}) = \Omega/Pe$ , the modulation frequency scaled by the convective time since we found that this choice facilitates the interpretation of the results.

As shown in Refs. 19 and 20 the flow is best described by the following two dimensionless parameters:

$$\delta = \frac{1}{W_1 - W_2} + \frac{1}{W_1 + W_2} \quad \text{and} \quad W_{\max} = W_1 + W_2,$$

their significance being that  $W_{\max}$  gives the largest contribution of  $\psi^E$  to the flow over one cycle and  $\delta$  measures the distance from the origin to the stagnation disk separating the two vortices.

The algorithm for calculating the enhancement factor  $\alpha$  was outlined in Sec. IV. We recall that this quantity is a function of time when a harmonic flow is considered, and this is illustrated in Fig. 6 for some specific values of  $W$ ,  $\delta$ , and  $Pe$ . In order to have a meaningful definition for  $\alpha$ , we define the average over the  $k$ th period,

$$\bar{\alpha}^k = \frac{1}{N_p N_p(k-1)+1} \sum_{N_p(k-1)+1}^{N_p k} \alpha^n,$$

where  $N_p$  is the number of time steps in a single period. We terminate the calculations for the first number  $k = K$  for which

$$\|\bar{\alpha}^{K+1} - \bar{\alpha}^K\| < 10^{-7} \quad \text{and then take} \quad \alpha = \overset{\text{def}}{\bar{\alpha}^{K+1}}.$$

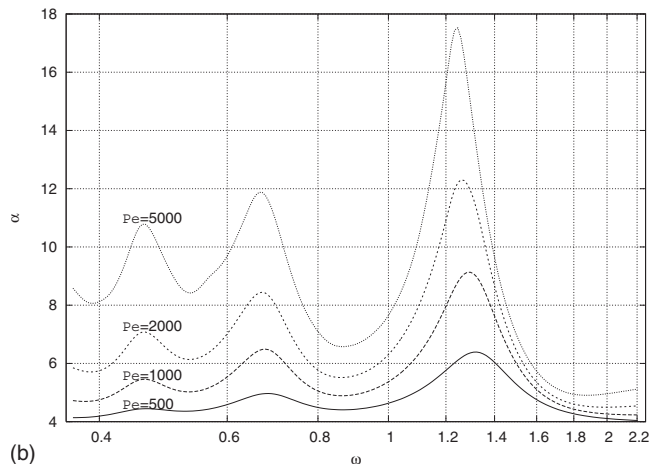
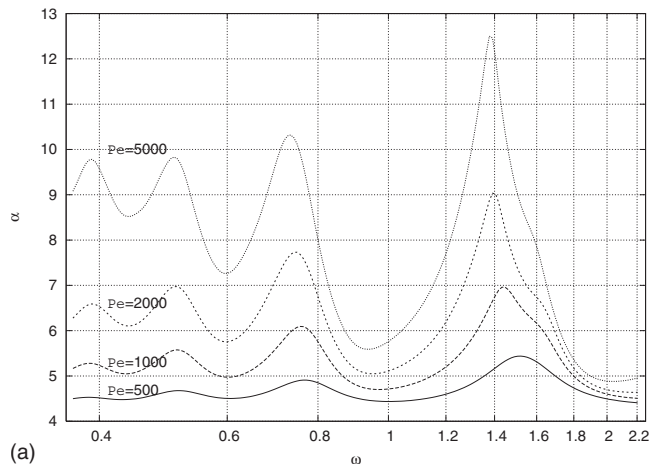


FIG. 7. The enhancement factor for  $\delta=4$  and different Pe. (a)  $W_{\max}=5$  and (b)  $W_{\max}=2$ .

The results for  $\alpha$  are shown in Figs. 7–9. Surprisingly, the computations show that the enhancement factor is a strongly nonmonotonic function of the frequency, exhibiting maxima and minima: We refer to the former as “resonances.” Although similar resonances have been observed in time-modulated spatially periodic flows,<sup>10,11</sup> their occurrence in closed recirculating flows is, with the exception of the lim-

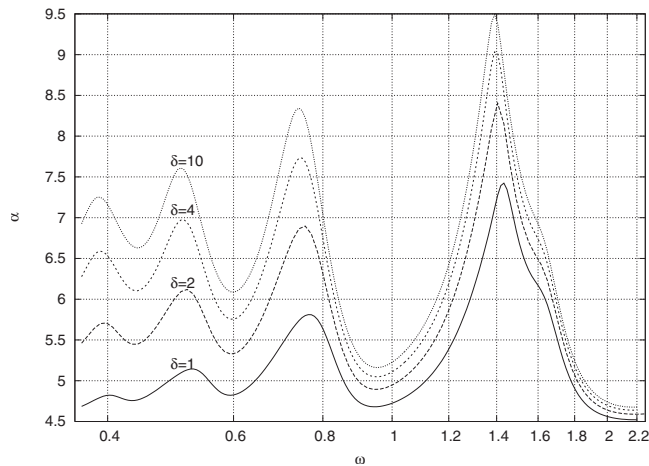


FIG. 8. The enhancement factor for  $Pe=2000$  and  $W_{\max}=5$  and different  $\delta$ .

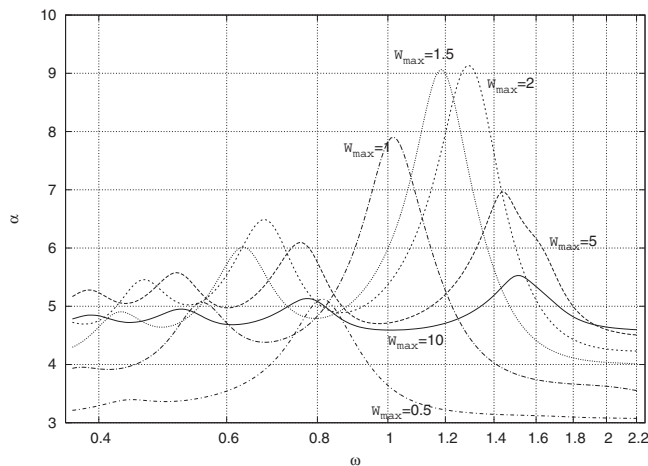


FIG. 9. The enhancement factor for  $\delta=4$  and different  $W_{\max}$  and  $Pe=1000$ .

ited results in Ref. 18, new. Thus the structure shown in Figs. 7–9 is unexpected and the reasons for it are not obvious. A conspicuous trait of the results is that the tallest peak resembles a cusp. For one set of parameters we took a much denser set of  $\omega$ -values in the vicinity of the spike in order to investigate the matter and we found that there is a smooth maximum but that the curvature is very large.

**B. The role of Pe**

We first examine the dependence of the enhancement factor on Peclet number for fixed  $\delta=4$ . Figure 7(a) presents the result for  $W_{\max}=5$ . At very high frequencies there is no effect of modulation on the extraction rate and the value of  $\alpha$  is the same as for the unmodulated case for these particular values of  $\delta$  and  $W$ . One clearly sees that there are some “resonant” frequencies for which the extraction is much faster than for the steady combined flow. The fact that these peaks are at the same nominal frequencies, independent of Pe, illustrates the reason for our scaling of the frequency and strongly suggests that a convective mechanism is responsible. One also sees that the influence of Peclet number is different for small ( $\omega < 0.8$ ) and large ( $\omega > 1$ ) frequencies. In all cases there is a very strong maximum at the upper end of the frequency interval. Beyond  $\omega=2$ , the fact that the flow is oscillatory has a negligible influence on the extraction rate. For very large and relatively small  $\omega$  nothing essentially new happens to the process. Figure 7(b), for  $W_{\max}=2$ , shows similar behavior, indicating the generality of the phenomenon. The qualitative behavior is the same: Only the amplitudes of the peaks are higher.

The position of the peaks is a very weak function of Pe: The relative position of the first two from the right suggests a subharmonic progression, but this is not borne out by the positions of the others. Similar trends, but for a very limited set of results, were observed by Lee *et al.*<sup>18</sup>

The value of  $\alpha$  for small  $\omega$  increases roughly as  $Pe^{1/3}$  while the asymptote for the large  $\omega$  is affected only slightly by Pe, consistent with Fig. 3. The height of the tallest peak also scales roughly as  $Pe^{1/3}$ . However, there is also a qualitative difference as the peak becomes very sharp with in-

creasing  $Pe$ . This means essentially that the dependence on  $Pe$  is not just of simple scaling: Rather,  $Pe$  influences the intrinsic mechanism of the resonance.

### C. The role of $\delta$

To investigate the dependence on  $\delta$  we choose  $W_{\max}=5$ . Figure 8 presents our results, in which the influence of  $\delta$  is seen to be straightforward: Larger  $\delta$  results in more effective extraction while the minima and maxima occur for virtually the same frequencies. We can conclude that in this range of  $\omega$ , the primary effect of  $\delta$  is to determine the magnitude of  $\alpha$  and that the low-frequency range is more susceptible to changes in  $\delta$  than the high-frequency range.

The increase in the enhancement factor with  $\delta$  is a very important physical result. Larger  $\delta$  means that the oscillatory flow accounts for a larger component of total the flow. (Recall that  $\delta=0$  is steady Hadamard–Taylor flow while for  $\delta \rightarrow \infty$  the oscillatory and stationary components of the flow are of nearly equal magnitude.) In other words, the excursions between the flow structures shown in Fig. 1 is larger for larger  $\delta$ , and it is not surprising that the enhancement factor increases monotonically with the magnitude of this excursion.

### D. The role of $W_{\max}$

The dependence of  $\alpha$  on  $W_{\max}$  is an intricate one. Whereas an increase in  $Pe$  or  $\delta$  led to an increase in the enhancement factor with all the other parameters fixed, the dependence on  $W_{\max}$  is complicated. As an example, Fig. 9 shows the enhancement factor as function of frequency  $\delta=4$ ,  $Pe=1000$ , and  $W_{\max}$  ranging from 0.5 to 10. The positions of the maxima are displaced for different  $W_{\max}$  which means that the intrinsic mechanisms of the resonance are strongly affected not only by the amplitude of excursion of the stagnation disk (parametrized by  $\delta$ ) but also by its mean position (parametrized by  $W_1 \approx \frac{1}{2}W_{\max}$ ). At the same time the amplitudes of the peaks are not monotonic functions of  $W_{\max}$ , which is the most distinctive feature of the results.

We investigated the dependence of  $\alpha$  on  $W_{\max}$  and  $Pe$  by first creating an extensive data set for a much wider range of  $W_{\max}$ ,  $Pe$ , and  $\omega$  than shown in Fig. 9 and then trying different scalings of the data. We found the for small  $W_{\max}$ ,  $\alpha$  scales with  $W_{\max}^{-1/3}$  and that it depends on the product  $W_{\max} Pe$  rather than on  $W_{\max}$  and  $Pe$  separately. Figure 10(a) shows how the results from this larger data set collapse using these rescalings.

In the other extreme of very large  $W_{\max}$  the scaling is qualitatively different: The position of the minima and maxima virtually do not depend on  $W_{\max}$  provided that the ratio  $Pe/W_{\max}$  is kept constant. Figure 10(b) shows the results in these rescaled variables for the large data set for large  $W_{\max}$ . We interpret this last result as follows. Recall that for large  $W_{\max}$  the characteristic velocity  $\bar{U} \approx UW_{\max}$ : Hence  $Pe/W_{\max}$  is the Peclet number of the Hadamard flow and it is reasonable to expect that this is the controlling parameter. Then the meaning of the ratio  $Pe/W_{\max}$  being constant is that enhancement factor depends linearly on  $Pe$ . This is in contrast with the case of steady flow where there is a satu-

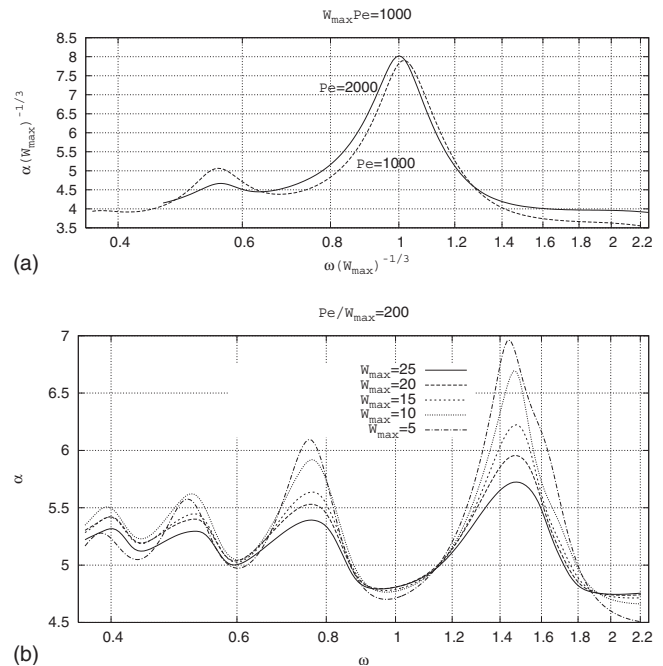


FIG. 10. The behavior of the enhancement factor for combinations of  $Pe$  and  $W_{\max}$  for  $\delta=4$ : (a) small  $W_{\max}$  and (b) large  $W_{\max}$ . (a) Small  $W_{\max}$ ,  $W_{\max} Pe=1000$  and (b) large  $W_{\max}$ ,  $Pe/W_{\max}=200$ .

ration of the enhancement factor at large Peclet number. If one could proceed to infinite Peclet numbers, the same kind of saturation is to be expected in the pulsatile case too, but this regime cannot be accessed numerically. With the results at hand one can conclude that  $Pe \approx 1000$ – $2000$  is still an intermediate Peclet number as far as the pulsatile flow is concerned.

## VII. MECHANISMS OF ENHANCEMENT: INVARIANT STRUCTURES AND PHASE LOCKING

As we have seen, the results for the modulated flow exhibit resonant peaks in plots of  $\alpha$  versus  $\omega$ . This observation strongly implies some kind of resonant interaction between the transport, the convective circulations within the drop, and the frequency of their modulation, but the details of the mechanism by which this interaction is produced remains in question.

Great insight into this question was obtained by producing and viewing movies of the concentration fields as a function of time. If the flow is steady, then of course the isopleths quickly conform to the streamlines within a few circulation times, reaching the typical configuration shown in Fig. 5, and thereafter decaying exponentially in time. In the modulated case, the concentration fields are convolutions of a time-periodic field and an exponential decay in time. We elucidated and visualized the time-periodic part in the following way: At any given time step, the isopleths were renormalized to a maximum value of unity and then displayed. In this way, we observed that the normalized spatial distributions of concentration were exactly repeated over each period, that is to say, the time-modulated part of the field is characterized by an underlying invariant time-periodic structure or a strange eigenmode.<sup>12,15</sup> The movies also helped to explain the role of

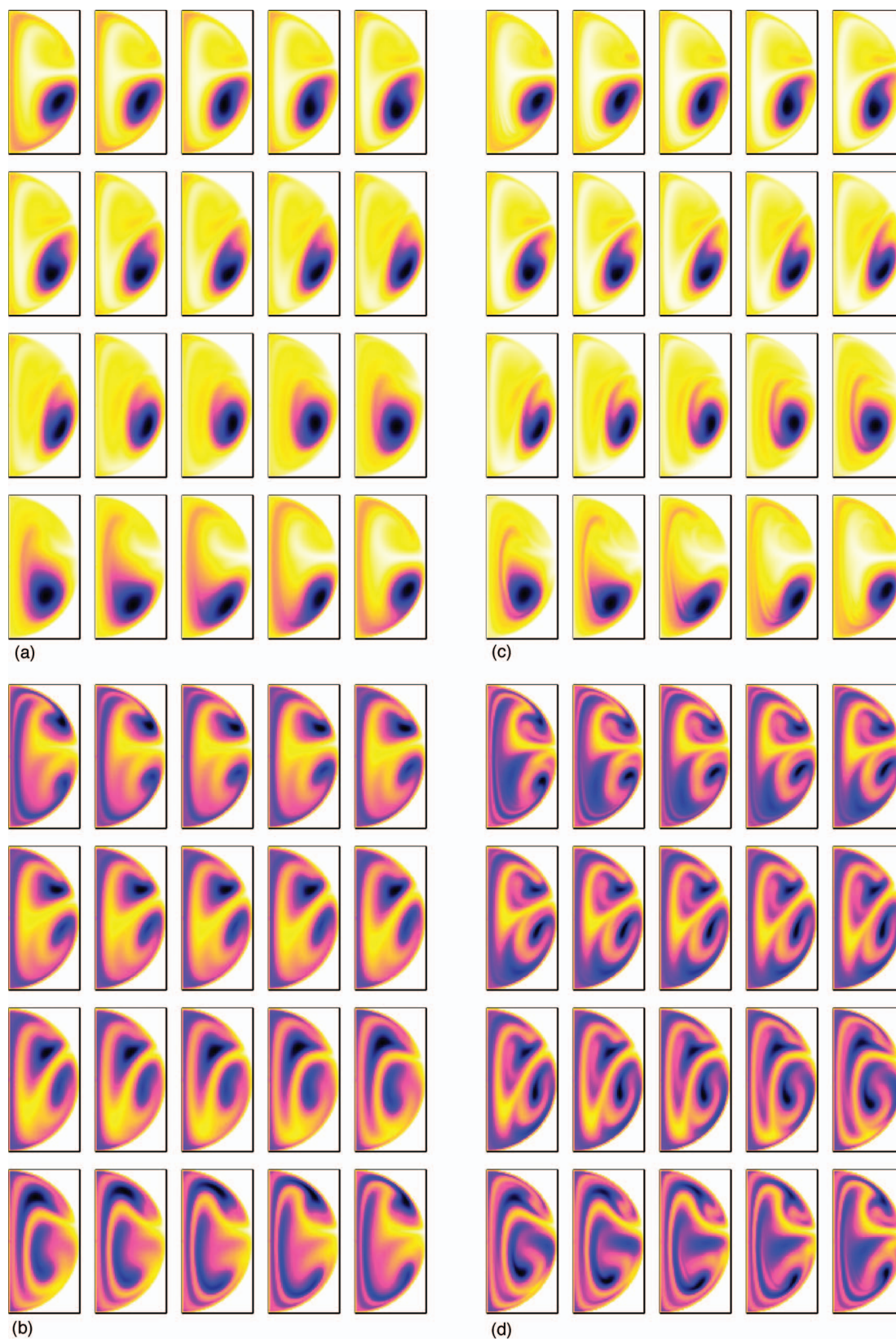


FIG. 11. (Color) Still frames (movies) of the concentration field as a function of time for  $\delta=4$ ,  $W_{\max}=2$ . (a)  $Pe=2000$ ,  $\omega=0.86$  [URL: <http://dx.doi.org/10.1063/1.3179555.1>], (b)  $Pe=2000$ ,  $\omega=1.26$  [URL: <http://dx.doi.org/10.1063/1.3179555.2>], (c)  $Pe=5000$ ,  $\omega=0.87$  [URL: <http://dx.doi.org/10.1063/1.3179555.3>], and (d)  $Pe=5000$ ,  $\omega=1.25$  [URL: <http://dx.doi.org/10.1063/1.3179555.4>] (enhanced online).

these time-periodic structures in enhancing the transport rates. We mention that the phenomena to be described are robust, occurring between each pair of peaks and valleys and over the entire range of parameters. These features are easi-

est to understand by viewing the movies, available in the online version of this paper, but can also be appreciated through a sequence of stills. Figure 11 shows two such sequences (movies in the online version) for  $\delta=4$ ,  $W_{\max}=2$  and

$\omega=0.86$  and  $1.25$  for  $Pe=2000$  and  $5000$ , respectively. In the stills, time runs left to right, top to bottom. These two particular values of  $\omega$  correspond to the last valley and the last large resonant peak in Fig. 7(b). The sequences of stills in Fig. 11 represent one period and show the invariant spatial structure that repeats indefinitely while decaying exponentially. Those readers studying the sequence of stills as opposed to viewing the movies should imagine them being “looped” from bottom to top. In interpreting these visualizations, it is good to recall that they are the result of convection and diffusion at high Peclet number in the presence of a flow consisting of a pair of toroidal vortices whose magnitude and location are modulated in time. These flows have nearly constant vorticity near their centers and straining flows near the equator, the poles, and the central axis, as shown, for example, in Figs. 1(b) and 1(c).

Beginning with the first panel of any sequence, it is seen that high concentration fluid is convected into two “blobs” near the vortex centers, and that these become well organized between panels 1 and 5. In the remainder of the cycle, these blobs are propelled toward the axis of the drop as a consequence of the relative strengthening and weakening of the Taylor flow. As they do, they find themselves in a flow field that has significant extensional character, as opposed to the primarily rotational flow near the vortex center, and as a result, striations or filaments of high concentration fluid are elongated, folded, and then convected along the interface. This process of filamentation, folding, and convection results in a higher concentration gradient at the interface than would otherwise be the case, leading in general to an enhancement of the mass transfer rate. This process is most pronounced in frames 11–20 of any of the sequences, and as already explained, repeats itself indefinitely.

While the occurrence of these structures can be anticipated from earlier works,<sup>12,15</sup> it remains to explain the resonant peaks. This paragraph describes the dynamics as interpreted from the stills: The same phenomena may be observed more readily by viewing the movies. The primary difference in the enhancement factors between the peaks and valleys is due to the temporal phase relationship between two blobs of the invariant strange eigenmode. In the valleys, typified by  $\omega=0.86$  and shown in Figs. 11(a) and 11(c), the two blobs are more or less in phase. This has two consequences: First, the highest concentration fluid is in the larger of the two blobs (as a result of its size), and second, there is little convective transport between the two blobs since they move nearly in phase with each other. In strong contrast, at resonant peaks, typified by  $\omega=1.25$  and shown in Figs. 11(b) and 11(d), the motion of the blobs toward the axis is *out of phase*. As a result, the filamentation is strikingly more pronounced and there is substantial convective exchange between them: Higher concentration fluid that begins the cycle in one blob finds itself in the other. In order to appreciate the differences between these two scenarios, compare frames 11–20 for the two frequencies for either value of  $Pe$ . This stronger degree of filamentation and more effective mass exchange leads in turn to much larger concentration gradients at the interface and is therefore responsible for the enhancement of the transport at these resonant peaks. Comparing Figs. 11(b) and

11(d), it is seen that the same phenomena occur for the two different values of  $Pe$ . However, since diffusion is weaker the higher the  $Pe$ , the concentration gradient is sharper for the larger  $Pe$ , leading to a relatively larger enhancement factor.

In this manner, we come to understand that the maximum enhancement is not due to a simple resonance between the driving frequency of the flow and a characteristic fluid circulation time, as has been suggested in literature on dynamical systems.<sup>10,11</sup> Rather, it is the *temporal phase relationship* between the two toroidal blobs of high concentration in the underlying strange eigenmode that determines the degree of enhancement.

## VIII. DISCUSSION AND CONCLUSIONS

We have examined mass (or heat) transport from a falling drop subject to an oscillating electric field when the internal phase resistance controls the transport. Our primary objective was to provide as complete picture of the transport as possible for both steady and unsteady flows. The flow field inside the drop is a superposition of a steady Hadamard and steady and oscillating Taylor flows. Accordingly, the problem is governed by four dimensionless parameters: a Peclet number  $Pe$  giving the importance of convection to diffusion;  $\omega$ , the frequency of the modulation made dimensionless using a characteristic convective time; and two parameters  $W_1$  and  $W_2$  representing the ratios of the steady and unsteady Taylor flows to the Hadamard circulation, respectively.

We use a high resolution finite-difference scheme to compute the concentration field. Following Kronig and Brink,<sup>1</sup> we characterize the transport rate in terms of the rate of decay of the total mass of solute in the drop, and we define the enhancement factor as the ratio of the decay rate to that for a stagnant drop.

We investigated the enhancement factor for steady flow as a function of the Peclet number for a wide range of values of the parameter  $W_1=W$ . Our primary result for steady flows is given in Fig. 3, where the curve  $W=0$  completes the classical Kronig–Brink problem. The general trend is in agreement with the extrapolated curve of Johns and Beckmann<sup>2</sup> and the results compare well with those of Bryden and Brenner,<sup>3</sup> who used a slightly different interfacial boundary condition and covered a smaller range of  $Pe$ .

Chang *et al.*<sup>5</sup> were the first to suggest an enhancement due to the presence of two toroidal vortices, but with the exception of some extremely limited results of Carleson and Berg, Fig. 7 of Ref. 7, this problem remained unsolved. When  $W \neq 0$  and the Peclet number is scaled as discussed in the text, there is a monotonic increase in  $\alpha$  with both  $W$  and  $Pe$ . With the exception of the very limited results for  $W=1$  and  $2$ ,  $Pe=50$  inferred from Fig. 7 of Carleson and Berg<sup>7</sup> (which agree with ours), these results are new and complete the solution for the steady problem. We found that Peclet numbers  $Pe \geq 200$  are asymptotically large as far as the extraction rate is concerned since in that range the extraction rate is virtually independent of  $Pe$ . The dependence on  $W$  is very strong for small  $W$  and for  $W > 8$  the results coincide

with the extraction rate for pure Taylor flow ( $W \rightarrow \infty$ ), for which the maximum enhancement factor of  $\alpha \approx 4.5$  is reached. Thus, although the transport remains diffusion limited as expected on general grounds, the enhancement can be very significant since the enhancement factor refers to the exponential decay rate.

Turning now to the case of modulated flow, we defined the enhancement factor as its average over one period and conducted extensive parametric studies in the four-dimensional space  $(\omega, Pe, W_1, W_2)$  or equivalently,  $(\omega, Pe, \delta, W_{\max})$ . We found the following results:

- a coherent picture which emerges only when the frequency is scaled by a convective time;
- invariant concentration fields (strange eigenmodes) that underlie the transport;
- resonant peaks that occur in plots of  $\alpha$  versus  $\omega$ ;
- no effect of modulation on the enhancement factor for large  $\omega$ ; and
- complicated scaling relations between the enhancement factor and the parameters  $(\omega, Pe, \delta, W_{\max})$ .

Some of these results remain unsupported by analytical understanding, but many may be understood along the following lines. The fact that the time scale for the frequency is a convective one indicates that it is the ratio of the modulation period to a typical circulation time that is important. The presence of several maxima and minima in the enhancement factor as a function of  $\omega$  was unexpected. To our knowledge, the only work suggesting the occurrence of multiple maxima is that of Fig. 10 of Lee *et al.*<sup>18</sup> Quantitative comparison between that work and ours is difficult since their results do not cover a wide range of parameters and the definitions of enhancement and the origin of the steady settling velocity component are different between the two works. However, we do not find that the resonant peaks are in the ratio of any simple rational fraction, as they suggest. The magnitude of  $\alpha$  at the maxima increases with increasing frequency and, after the highest peak, decays rapidly to a limited value. Thus, for large frequencies (somewhat larger than 2.0) there is no appreciable enhancement compared to the steady Hadamard–Taylor flow. A complete study of very low frequencies lies beyond the scope of the present work. However, we did some exploratory calculations in that region and in all cases we discovered a linear dependency of  $\alpha$  on  $\omega$  below  $\omega \approx 0.1$ – $0.2$ . Thus the frequency dependence for large and small  $\omega$  conforms to the general expectations developed in other contexts.<sup>8,9</sup> The origin of these resonant peaks turned out to be complex and subtle, as revealed by movies of the concentration field, examples of which are given in Figs. 11(a)–11(d). As explained in Sec. VII, the peaks occur as a

result of phase locking between the two oscillatory blobs of high concentration fluid in the underlying invariant spatial structure.

## ACKNOWLEDGMENTS

This work was supported by grants to G.M.H. from the U.S. DOE, Office of Basic Energy Sciences (Grant No. DOE/DE-FG02-05ER15692) and the Microgravity Sciences Program of NASA (Grant No. NNC04GA42G), and from the Board of Regents of Louisiana through Grant No. RD-B-09 for C.I.C. (2004–2005).

- <sup>1</sup>R. Kronig and J. C. Brink, “On the theory of extraction from falling droplets,” *Appl. Sci. Res. A* **2**, 142 (1951).
- <sup>2</sup>L. E. Johns, Jr. and R. B. Beckmann, “Mechanism of dispersed-phase mass transfer in viscous, single-drop extraction systems,” *AIChE J.* **12**, 110 (1966).
- <sup>3</sup>M. D. Bryden and H. Brenner, “Mass-transfer enhancement via chaotic laminar flow within a droplet,” *J. Fluid Mech.* **379**, 319 (1999).
- <sup>4</sup>Y.-F. Pan and A. Acrivos, “Heat transfer at high Peclet number in regions of closed streamlines,” *Int. J. Heat Mass Transfer* **11**, 439 (1968).
- <sup>5</sup>L. Chang, T. E. Carleson, and J. C. Berg, “Heat and mass transfer to a translating drop in an electric field,” *Int. J. Heat Mass Transfer* **25**, 1023 (1982).
- <sup>6</sup>G. I. Taylor, “Studies in electrohydrodynamics. I. The circulation produced in a drop by electric field,” *Proc. R. Soc. London, Ser. A* **291**, 159 (1966).
- <sup>7</sup>T. E. Carleson and J. C. Berg, “Marangoni and electric field effects upon mass transfer to translating drops,” *Chem. Eng. Commun.* **25**, 117 (1984).
- <sup>8</sup>V. Rom-Kedar and A. C. Poje, “Universal properties of chaotic transport in the presence of diffusion,” *Phys. Fluids* **11**, 2044 (1999).
- <sup>9</sup>V. Rom-Kedar, “Frequency spanning homoclinic families,” *Commun. Nonlinear Sci. Numer. Simul.* **8**, 149 (2003).
- <sup>10</sup>T. H. Solomon and I. Mezić, “Uniform resonant chaotic mixing in fluid flows,” *Nature (London)* **425**, 376 (2003).
- <sup>11</sup>T. H. Solomon, A. T. Lee, and M. A. Foglerman, “Resonant flights and transient superdiffusion in a time-periodic, two-dimensional flow,” *Physica D* **157**, 40 (2001).
- <sup>12</sup>R. T. Pierrehumbert, “Tracer microstructure in the large-eddy dominated regime,” *Chaos, Solitons Fractals* **4**, 1091 (1994).
- <sup>13</sup>G. Voth, G. Haller, and J. P. Gollub, “Experimental measurements of stretching fields in fluid mixing,” *Phys. Rev. Lett.* **88**, 254501 (2002).
- <sup>14</sup>D. Rothstein, E. Henry, and J. P. Gollub, “Persistent patterns in transient chaotic fluid mixing,” *Nature (London)* **401**, 770 (1999).
- <sup>15</sup>G. Haller and W. Liu, “Strange eigenmodes and decay of variance in the mixing of diffusive tracers,” *Physica D* **188**, 1 (2004).
- <sup>16</sup>E. Saadjan and L. C. Leprevost, “Chaotic transfer in a periodic two-dimensional flow,” *Phys. Fluids* **10**, 2102 (1998).
- <sup>17</sup>T. J. Kaper and S. Wiggins, “An analytical study of transport in Stokes flows exhibiting large-scale chaos in the eccentric journal bearing,” *J. Fluid Mech.* **253**, 211 (1993).
- <sup>18</sup>S. M. Lee, D. J. Im, and I. S. Kang, “Circulating flows inside a drop under time-periodic nonuniform electric fields,” *Phys. Fluids* **12**, 1899 (2000).
- <sup>19</sup>T. Ward and G. M. Homsy, “Electrodynamically driven chaotic mixing in a translating drop,” *Phys. Fluids* **13**, 3521 (2001).
- <sup>20</sup>T. Ward and G. M. Homsy, “Electrodynamically driven chaotic mixing in a translating drop. II. Experiments,” *Phys. Fluids* **15**, 2987 (2003).
- <sup>21</sup>G. I. Marchuk, *Methods of Numerical Mathematics* (Springer-Verlag, New York, 1975), Vol. 4.
- <sup>22</sup>J. F. Patzer II and G. M. Homsy, “Global stability of transient drop extraction to Marangoni instabilities,” *Phys. Fluids* **24**, 567 (1981).